# Bundling dynamics of single walled carbon nanotubes in aqueous suspensions

Goki Eda,[a] Giovanni Fanchini, Alokik Kanwal, and Manish Chhowalla[a]
*Materials Science and Engineering, Rutgers University, 607 Taylor Road, Piscataway, New Jersey 08854, USA*

(Received 8 January 2008; accepted 6 March 2008; published online 15 May 2008)

A simple optical method based on absorption of monochromatic light to investigate the dynamics of single walled carbon nanotube (SWCNT) suspensions is described. The well dispersed suspensions display a complex behavior, exhibiting peaks due to resonant scattering from SWCNT bundles with increasing diameters as a function of time. The results indicate that the bundling of SWCNTs initiates almost immediately after termination of sonication (after ~0.1 h) and continues to increase up to a critical time (~10 h), above which precipitation according to the Stokes relationship occurs. The absorbance behavior can be explained by the depletion of the effective medium as well as the Mie scattering from growth of bundles. A semiquantitative analysis of the experimental data based on the Mie theory of light scattering from cylindrical particles allows the extraction of diameters at the nucleation and growth of SWCNT bundles. The bundling dynamics have been correlated with the electrical properties such as the sheet resistance and transistor characteristics of the SWCNT thin films. Our work is a useful step toward reproducible solution processed electronics because it provides a simple method to monitor the quality of SWCNT suspensions in real time and correlate it to device characteristics. © *2008 American Institute of Physics*. [DOI: 10.1063/1.2919164]

## I. INTRODUCTION

Networks of single walled carbon nanotubes (SWCNTs) are interesting electronic materials that have opened a route to a new class of thin film devices.[1] While individual SWCNTs have been considered as ideal building blocks for nanoelectronics, the intense effort required to disperse,[2] separate,[3] and manipulate them have limited their implementation in electronic devices. In contrast, SWCNT thin film electronics takes advantage of ease of processing because it does not require intense molecule-level manipulation. SWCNT thin films can either be directly grown onto substrates at high temperatures (700–900 °C) or more preferably deposited from solution. Solution processing is particularly important for the emerging field of printable electronics where the components of the device can be deposited from suspension or "inks" consisting of nanoparticles in solvents by using inkjet or roll-to-roll printing onto inexpensive and flexible substrates.[4–8] Promising results for applications in transparent and conducting electrodes,[9–11] thin film transistors[12,13] (TFTs), optoelectronic devices,[14–16] and chemical sensors[17] have been reported for a variety of solution processed materials.

In order for solution processed SWCNT thin film electronics to be viable, it is crucial that devices with consistent performance be fabricated. One of the primary limitations to reproducibility of SWCNT thin film devices is the occurrence of bundling in suspension or during deposition. Bundling is detrimental for the optoelectronic properties of SWCNT thin films due to an increase in surface roughness and also their large optical cross section. In addition, bundles are metallic[18] and therefore give rise to a large off current in SWCNT TFTs.[12] Furthermore, since bundling often occurs in a nonrepeatable manner, it manifests as nonreproducible characteristics in SWCNT thin film devices. Therefore, real time monitoring of the bundling dynamics in SWCNT suspensions is critical for fabrication of devices with reproducible properties. However, the dynamics of SWCNT bundle formation in suspensions are not clearly understood. While various spectroscopic[19–22] and scattering[23–25] techniques may be used to infer the aggregation state of SWCNTs, bundling kinetics in solution are difficult to probe due to complications introduced by sedimentation[26] and diffusion.[25]

In this study, we describe a simple method to monitor the settling behavior of SWCNTs in aqueous suspensions. The method involves monitoring the absorbance of the suspension at three different heights as a function of time. For well dispersed suspensions, the absorbance was found to be constant for the first ~0.1 h, after which modulations in the data appeared. Specifically, since our atomic force microscopy (AFM) and scanning electron microscopy (SEM) studies of SWCNT bundle sizes from samples taken from the suspensions reveal diameters ranging from a few nanometers up to the order of the wavelength used to measure the absorbance, we show that the modulations can be correlated with resonances predicted by the Mie theory of light scattering from cylindrical nanoparticles. It should therefore be noted that here, the term absorbance refers to attenuation of light by two phenomena: light scattering and absorption effects within the particles. A semiquantitative interpretation of our absorbance data reveals that the aggregation of SWCNTs in the suspension is a highly dynamic process in which an increase in the bundle size occurs upon termination of sonication. According to our observations, gradual bundling takes

[a]Authors to whom correspondence should be addressed. Electronic mail: goki@eden.rutgers.edu and manish1@rci.rutgers.edu.

 

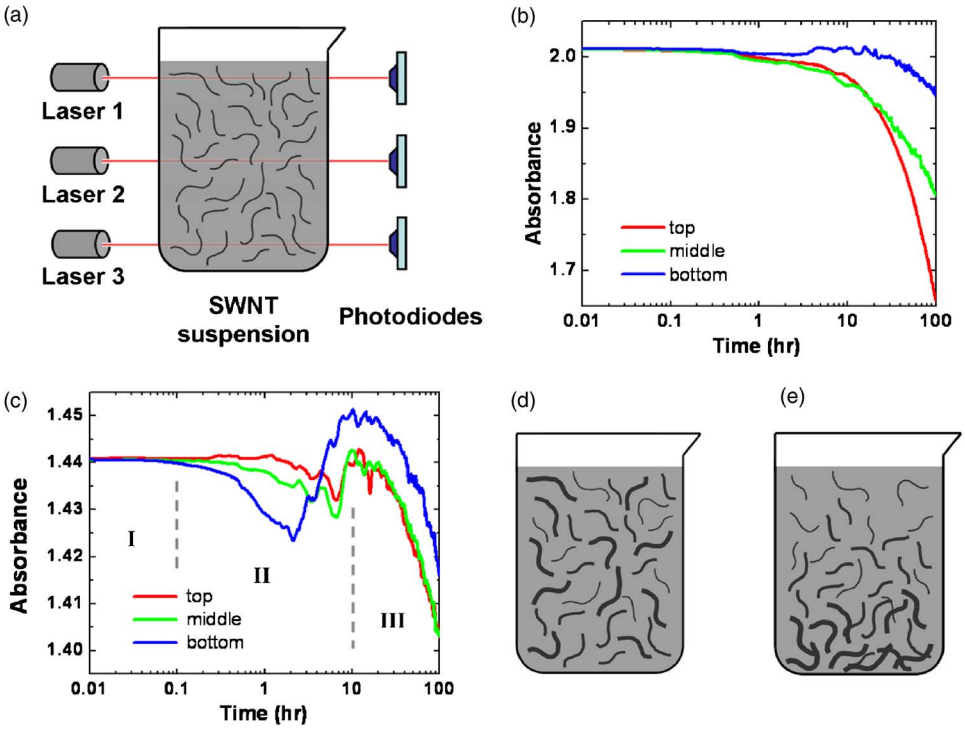


FIG. 1. (Color online) (a) Schematic of the measurement apparatus. Three red lasers ($\lambda$=655 nm) and photodiodes were used to measure the absorbance of the SWCNT suspension at three different levels. Measured absorbance as a function of time for (b) poorly dispersed and (c) well dispersed suspensions. Three settling regimes for well dispersed suspensions are indicated by Roman numerals (see text). Evolution of the state of the SWCNT suspension is depicted in (a), (d), and (e). Initially (a) well dispersed SWCNTs (d) aggregate into bundles and subsequently (e) precipitate to the bottom with progressing settling time.

place until a critical mass is reached (at ~10 h of settling time) when the bundles precipitate. At longer settling times, precipitation of the bundles continue while lighter particles with little tendency to aggregate, presumably individual SWCNTs, or very small bundles, remain in suspension. Finally, to correlate the dynamic behavior of SWCNT suspensions to electronic characteristics, we have measured the electrical properties of thin films from SWCNTs sampled at various times from the center of the vessel. We found that the sheet resistance of the SWCNT thin films decreased with settling time, reaching a minimum at ~10 h and subsequently increased to approximately the same value as SWCNT thin films deposited from freshly sonicated solutions. The on/off ratio of the SWCNT TFTs was also found to follow a similar trend.

## II. METHODS

SWCNTs synthesized by high-pressure catalytic decomposition of carbon monoxide (HiPCO) purchased from Carbon Solutions, Inc. and thoroughly purified by a process described elsewhere[27] were used in this study. Purified SWCNTs were solubilized in an aqueous solution of 1 wt % sodium dodecyl sulfate (SDS) at a concentration of 2 mg/l. Prior to performing the absorbance measurements, the SWCNT suspensions were homogenized by bath sonication for 2 h to achieve a uniform ink. An additional SWCNT suspension of 1 wt % SDS and methanol was also investigated for comparison. The dispersion stability of the methanol containing suspension is poor because methanol has a strong affinity for SDS and causes the surfactant to desorb from the SWCNTs,[6] promoting rapid bundling. The bundling dynamics and dispersion stability of the two suspensions were investigated by monitoring the absorbance of a red diode laser ($\lambda$=655 nm) with photodiodes at three different heights (top, middle, and bottom) of the vessel, as schematically shown in Fig. 1(a). The absorbance at the three levels was recorded every 5 s for over 100 h immediately starting after sonication.

## III. SETTLING OF SWCNT SUSPENSIONS

The measured absorbance values as a function of time for the two suspensions are plotted in Figs. 1(b) and 1(c). The data for the methanol containing suspension shown in Fig. 1(b) follow an expected trend for suspensions of heavy particles. In such systems, a sedimentation of bundles of varying masses with different Stokes velocities results in the development of a concentration gradient from the top to the bottom of the suspension.[28] This is readily seen as decay in absorbance beginning from the top of the suspension. This type of settling behavior can be described by classical equations of motion as demonstrated by Nicolosi *et al.*[26] for sedimentation of MoSI nanowires. In this case, the absorbance with time generally remains constant for up to a critical time, after which it exponentially decays, as seen in Fig. 1(b), demonstrating that bundling takes place immediately upon the addition of methanol followed by sedimentation.

In contrast, the behavior of absorbance versus time data of the well dispersed suspension without methanol shown in Fig. 1(c) is more complex. Specifically, the absorbance remains relatively constant for all three laser positions up to ~0.1 h, above which it decreases and then increases again for several hours, giving rise to broad features at all three laser positions. Such features are more dramatic at the bottom of the vessel presumably due to a higher concentration of material from precipitation. Small modulations superimposed on the broad features can also be readily seen on each of the experimental absorbance curves. Subsequently, exponential decay similar to the methanol containing suspension

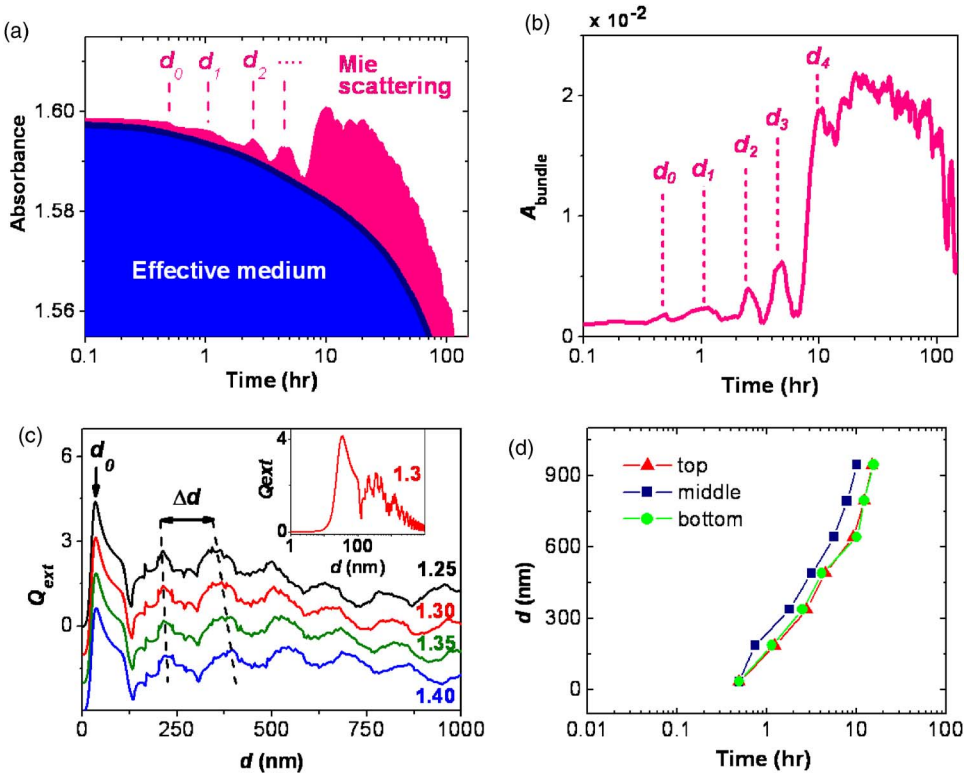


FIG. 2. (Color online) (a) Schematic of the model used for the interpretation of optical absorbance with time. The contribution of the small particles in a well dispersed suspension to the absorbance is represented by the blue curve as an exponential decrease in the absorbance due to the depletion of the effective medium. The contribution of the cross-sectional enhanced Mie scattering from bundles is represented by the resonance peaks shown in red. The Mie scattering peaks ($d_i$) are labeled on the red curve. (b) Replotted experimental absorbance versus time data with the contribution from the effective medium subtracted ($A_{bundle}=A_{total}-A_{indiv}$) for the middle laser to clearly identify the resonance peaks. (c) Enhanced cross-sectional $Q_{ext}$ vs bundle size for particles with $N_{\|}=1.7+i0.7$ and $N_{\|}=3.5+i2.5$ (realistic values for HiPCO SWCNTs) at various medium refractive indices. The initial particle size of the bundles ($d_0$) was calculated to be ~34 nm and each subsequent peak indicates the growth of the bundles by $\Delta d$. The curves for $N=1.3-1.4$ are offset for clarity. The inset emphasizes that no cross-sectional enhancement is present for particle sizes below ≈10 nm. (d) Summary of bundle diameters as a function of time extracted from the experimental results.

is observed after ~10 h. The anomalous behavior between ~0.1 and ~10 h can be attributed to the gradually increasing size and amount of SWCNT bundles. We will explain the origin of such broad peaks and also the smaller superimposed modulations in detail below.

Before launching into the theory, major features of the absorbance curves in Fig. 1(c) can be summarized in terms of three regimes. Regime I is the plateau up to around 0.1 h implying good dispersion dominated by individual SWCNTs and/or limited volume fraction of bundles. Regime II ($0.1<t<10$ h) is characterized by a broad dip and the subsequent increase in absorbance and appearance of small modulations arising from increasing bundle size. Finally, regime III ($t>10$ h) is characterized by exponential decay due to sedimentation of large bundles. These three regimes are schematically depicted in Figs. 1(a), 1(d), and 1(e), respectively.

## IV. INTERPRETATION OF SETTLING DYNAMICS

In order to obtain insights into the bundling dynamics and a physical picture of the mechanisms involved, we have performed a semiquantitative analysis of the experimental absorbance data. For the analysis, we assume that the measured absorbance of the suspension is a sum of two contributions such that $A_{total}=A_{indiv}+A_{bundle}$, where $A_{indiv}$ is the absorbance due to individual SWCNTs or very small bundles (few nanometers in diameter), and $A_{bundle}$ is the absorbance due to large bundles (few tens to hundreds of nanometers in diameter). Therefore, $A_{indiv}$ is primarily influenced by changes in the effective medium consisting of SWCNTs and SDS solution. This assumption is based on the fact that from our AFM analysis, SWCNT thin films prepared from the suspension typically contain a large fraction of well dispersed SWCNTs (bundles below ~10 nm in diameter) along with a small fraction of large bundles (>10 nm in diameter). The contribution of these two terms in measured absorbance is schematically described in Fig. 2(a) [actual data from Fig. 1(c) have been incorporated into the sketch to illustrate the modeled phenomena]. The illustration depicts the exponential decay in the effective medium (blue curve) as well as the modulations due to Mie scattering from increasing fraction of bundles with diameters close to being in resonance with the probing wavelength (red curve). For clarity and better interpretation of the contribution from large bundles, the decay in effective medium was modeled with a stretched exponential function and subtracted from the experimental absorbance data. The data for the middle laser in Fig. 1(c) after subtraction of the effective medium contribution is replotted in Fig. 2(b). Resonance peaks with varying intensities indicating increasing size and variable fraction of bundles can be

readily observed in Fig. 2(b). In Figs. 2(a) and 2(b), the peak positions are labeled as $d_0$, $d_1$, $d_2$, and so on, where $d_0$ is defined as the critical bundle size for the initial principal maximum and the modulations as $d_i$ $(i=1,2,3,\ldots)$. Below, we semiquantitatively explain our observations in terms of the cross-sectional enhanced Mie scattering from suspended cylindrical particles[29] and demonstrate how the peak positions in the experimental absorbance data can be used to obtain the size of particles in suspension.

### A. Mie scattering in SWCNT suspensions

Attenuation of electromagnetic waves incident on small particles with size comparable to the wavelength is particle-size dependent due to complex interference of scattered electromagnetic waves. The Mie theory provides analytical solutions to the Maxwell equations describing these complex phenomena.[29] Assuming SWCNT bundles as infinitely long cylindrical particles attenuating the laser beam, the Mie theory can be applied to model the origin of the observed peaks in Fig. 2(b).

Absorbance of a suspension consisting of cylindrical particles can be expressed as

$$A = \frac{fQ_{\text{ext}}}{\pi d}L, \tag{1}$$

where $f$ is the volume fraction occupied by the particles, $d$ is the particle diameter, $L$ is the width of the vessel containing the solution, and $Q_{\text{ext}}$ is the extinction cross section that results from two distinct phenomena: absorption and scattering of incident light by the illuminated particles. Extinction cross section can be expressed as[29]

$$Q_{\text{ext}} = \frac{2}{x}\sum_{n=1}^{\infty}\text{Re}\left\{b_{0I}(x) + 2\sum_{n=1}^{\infty}b_{n\text{I}}(x) + a_{0\text{II}}(x) + 2\sum_{n=1}^{\infty}a_{n\text{II}}(x)\right\}, \tag{2}$$

where the harmonic coefficients $a_{n\text{II}}$ and $b_{n\text{I}}$ are related to the $n$th order solution of the Maxwell equations for an incident plane wave with boundary conditions determined by the geometry of the particles. These coefficients depend on the diameter of the particles and the refractive index $N$ of the background medium (aqueous solution with 1 wt % SDS) through the size parameter: $x=2\pi Nd/\lambda$. The $a_{n\text{II}}$ coefficients are related to absorption and scattering of incident radiation polarized perpendicular to the axis of the cylindrical particles, while the $b_{n\text{I}}$ coefficients are related to those of incident radiation polarized parallel to the particle axes. Therefore, for optically anisotropic cylinders, the $a_{n\text{II}}$ coefficients depend only on the out-of-axis refractive index of the particles $N_\perp$, while the $b_{n\text{I}}$ coefficients depend only on the in-axis refractive index of the particles $N_\parallel$,

$$a_{n,\text{II}} = \frac{C_n(M_\perp,\zeta,x)V_n(M_\perp,\zeta,x) - B_n(M_\perp,\zeta,x)D_n(M_\perp,\zeta,x)}{W_n(M_\perp,\zeta,x)V_n(M_\perp,\zeta,x) + iD_n(M_\perp,\zeta,x)^2},$$

$$b_{n,\text{I}} = \frac{W_n(M_\parallel,\zeta,x)B_n(M_\parallel,\zeta,x) + iD_n(M_\parallel,\zeta,x)C_n(M_\parallel,\zeta,x)}{W_n(M_\parallel,\zeta,x)V_n(M_\parallel,\zeta,x) + iD_n(M_\parallel,\zeta,x)^2}, \tag{3}$$

where $A_n$, $B_n$, $C_n$, $D_n$, $V_n$, and $W_n$ are quantities that, related to the $n$th order cylindrically symmetric Bessel and Hankel functions,[29] preserve information about the geometry of the particles. They depend on $M_\parallel=N_\parallel/N$ or $M_\perp=N_\perp/N$ and on the incidence angle $\zeta$. Except for the zeroth order solutions, both $a_{n\text{II}}$ and $b_{n\text{I}}$ tend to zero for sufficiently large values of $n$ and sufficiently low values of $x$. The evaluation of Eq. (2) can then be carried out by retaining a finite number of terms in the summation.[30] In order to determine $M_\parallel$ and $M_\perp$, the complex refractive indices of HiPCO SWCNTs recently reported by Fagan *et al.*[31] were used. The extinction cross section versus the bundle diameter was calculated[32] at several values of $N$ (near values for pure water $N=1.30$ at $\lambda=655$ nm) to account for possible changes in the refractive index of the aqueous medium.

### B. SWCNT bundle sizes

The results of our calculations for various values of $N$ are summarized in Fig. 2(c). The prominent $d_0$ peak arising from the nucleation of bundles of critical sizes is readily obtained as the initial principal maximum from the calculations. The intervals between the modulations in Fig. 2(c) represent the change in particle size $(\Delta d)$ with time. Thus, our calculations suggest that it is possible to obtain the sizes of the bundles with time from the intervals between the modulations in the experimental absorbance measurements [Fig. 2(b)]. It can be observed from Fig. 2(c) that for the most likely values of refractive index for water-SDS effective medium $(N=1.24-1.4)$, both $d_0$ and $\Delta d$ only weakly depend on $N$. The inset of Fig. 2(c) is an enlargement of the calculated results at low particle sizes to clearly indicate that there are no resonance peaks below $d_0$. The values of $d_0$ and $\Delta d$ were found to be 34 and 152 nm, respectively, for $N=1.3$. The results of our simulations suggest that during the time between two consecutive resonance peaks, bundle diameters increase by ~150 nm. The multiple peaks in the absorbance data [Fig. 2(b)] indicate the formation of large bundles, which is consistent with the fact that we occasionally find bundles of several hundred nanometers in the SWCNT thin films. Assuming that each resonance peak in Fig. 2(b) represents absorbance from the most prevalent bundles within the probed volume, the bundle size as a function of time can be extracted by utilizing $d_0$ and $\Delta d$, as shown in Fig. 2(d). The increase in the average bundle size within the probed volume at the three locations within the vessel can be readily seen in Fig. 2(d). Furthermore, it can also be concluded from Fig. 2(d) that the estimated bundle size at $t>10$ h is sufficiently large for sedimentation to occur according to the Stokes law. This correlates well with the onset of regime III in Fig. 1(c), where precipitation of bundles becomes significant. Therefore, the small modulations in Fig. 2(b) can be attributed to resonance while the broad increase in absorbance prior to the exponential decay can be attributed to the overall increase in the bundle con-

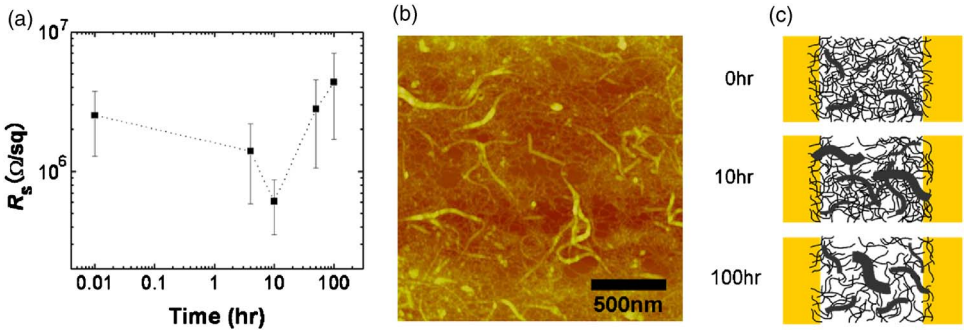


FIG. 3. (Color online) (a) Average sheet resistances ($R_s$) for SWCNT thin films prepared at different settling times. The minimum sheet resistance was found at settling times=10 hours. (b) Typical AFM image of the prepared thin film showing individual SWCNTs and bundles of few tens of nanometers in diameter can be readily observed. (c) Schematic of the SWCNT network showing different degrees of bundle percolation as a function of the settling time. The schematic shows bundles percolating across the network for a settling time of around 10 h, giving rise to minimum $R_s$.

centration. It should be noted that the small intensity of resonance modulations superimposed on the broad feature in Figs. 1(c) and 2(b) indicates that the fraction of large bundles is small compared to those of individual SWCNTs and small bundles ($<10$ nm in diameter).

## V. EFFECT OF BUNDLING ON THIN FILM ELECTRICAL PROPERTIES

In order to investigate the impact of the complex settling behavior on the electronic properties of SWCNT networks, thin films were prepared at different times after sonication. We define the time elapsed from sonication as "settling time" $t_s$. A small amount of suspension (3 ml) was carefully sampled from the center of the vessel at the same location for all measurements and diluted to 0.05 mg/l with 1 wt % SDS solution. It should be pointed out that bundling is greatly reduced due to a lower probability of bundle-bundle interactions through dilution. Debundling, which is an irreversible process,[20] is also unlikely. The diluted suspension was then vacuum filtrated to "freeze" the aggregation state into a two-dimensional structure. A filtration volume of 60 ml at this concentration was chosen to yield a low density film below the metallic percolation threshold.[33] Electrical properties were evaluated for SWCNT thin films deposited onto $SiO_2/p$-Si substrates with evaporated Au electrodes.

Electrical measurements were performed at different locations on the substrates to account for variations arising from fluctuations in tube density within the film. A large channel separation of 20 $\mu$m, which is much greater than the length of individual SWCNTs, was chosen to ensure that the transport was dominated by percolation.[34] The average sheet resistance ($R_s$) was found to reach a minimum at $t_s=10$ h, as clearly observed in Fig. 3(a). This time coincides with the end of regime II discussed earlier in the absorbance data [Fig. 1(c)], which corresponds to a maturing of bundle size before precipitation. A typical AFM image showing the range of bundle sizes in the SWCNT thin films deposited after a settling time of 10 h is shown in Fig. 3(b). The changes in $R_s$ in terms of degree of bundling can be qualitatively explained by considering percolation of metallic SWCNTs in bundles. That is, due to the high probability that a bundle contains several metallic SWCNTs, percolation among the bundles effectively acts as a long conducting channel. Gradual increase in $R_s$ for $t_s>10$ h corresponds with regime III of absorbance spectrum where the number of large bundles decreases at the center of the vessel due to sedimentation. The probability of metallic SWCNT percolation therefore diminishes, resulting in higher $R_s$. The distribution of bundles, giving rise to the trend in sheet resistance with time in Fig. 3(a), within the conducting channel as a function of the settling times is schematically summarized in Fig. 3(c).

Evidence for metallic SWCNT percolation was also found in TFT characteristics, as shown in Fig. 4. All of the devices examined in this study exhibited the typically observed $p$-type behavior,[12] as indicated by the transfer characteristics in Fig. 4(a). It should be noted that the measurements were made without the elimination of metallic

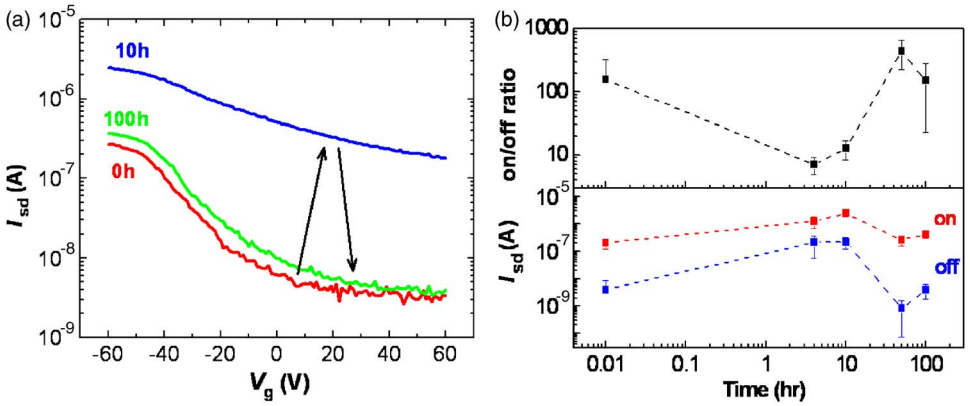


FIG. 4. (Color online) (a) TFT characteristics (source-drain current $I_{sd}$ as a function of gate voltage, $V_g$) of typical devices for thin films deposited at settling times of 0, 10, and 100 h. (b) Variation of on/off ratio and on and off currents for SWCNT TFTs prepared at different settling times. Leakage (off) current increases more than an order of magnitude during the initial 10 h giving rise to a low on/off ratio.

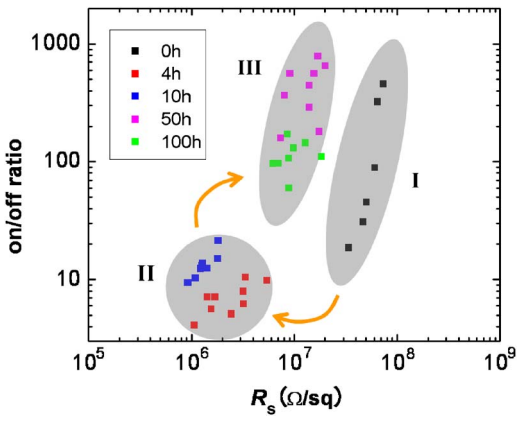


FIG. 5. (Color online) On/off ratio of each TFT device mapped against sheet resistance ($R_s$). The device characteristics mostly fall within the three shaded regions depending on the settling regime.

SWCNTs (Ref. 35) in order to understand the effect of bundles on device performance. We chose a large channel length ($L_c$=210 $\mu$m) in order to clearly observe the variations in the on/off ratio of the TFTs. The on/off ratios were found to depend on $t_s$, as shown in Fig. 4(b). As discussed by Kocabas *et al.*,[36] the on/off ratio of the SWCNT TFTs is sensitive to percolation of metallic SWCNTs, which gives rise to a large off-current. In this study, it is clearly seen that the on/off ratio is suppressed for films prepared in regime II ($t_s$=2–10 h), where large off-currents [Fig. 4(b)] are obtained due to the percolation of bundles. The higher fraction of bundles in the channel is the result of aggregation and precipitation to the middle of the vessel at these intermediate settling times. In regime III, the on/off ratio recovers by an order of magnitude due to the precipitation of large bundles, which is in agreement with the behavior of $R_s$.

We further observed that the variation of on/off ratio within each film is typically a function of $R_s$, as plotted in Fig. 5. It can be seen that the relationship between the on/off ratio and $R_s$ also changes with $t_s$. For example, while similar on/off ratios are achieved for regimes I and III, there is a distinct horizontal shift (change in $R_s$) in the two groups of data. The primary difference in the films prepared in these regimes is the amount of individual SWCNTs at the center of the vessel. In regime III, the number of individual SWCNTs is less compared to regime I due to bundling. This implies that the large number of cross junctions[37] present in films prepared during regime I may give rise to a larger $R_s$. In this respect, the relationship between the on/off ratio and $R_s$ may be a key in understanding the quality of the SWCNT network.

## VI. CONCLUSIONS

We have presented a simple optical method for diagnosing the bundling and sedimentation dynamics of SWCNTs in suspension. This method exploits resonances that arise from the Mie scattering of a laser beam by the SWCNT bundles with sizes comparable to the probing wavelength (thus in the range of a few tens to hundreds of nanometers). With this method, we determined that the bundle diameter rapidly increases with time as soon as agitation by sonication is terminated. We also showed that bundling and sedimentation dynamics in suspension give rise to significant variations in electrical properties of SWCNT networks. SWCNT thin films containing large bundles exhibit large off-current due to a high probability of metallic percolation paths present in the network. In order to obtain SWCNT thin films with reproducible properties, it is crucial that the state of suspensions is known. Improvement toward determining and maintaining highly dispersed and stable suspensions is essential for achieving SWCNT network devices with enhanced performance and reproducibility.

## ACKNOWLEDGMENTS

We acknowledge Steve Miller for help with SEM analysis. This work was funded by the National Science Foundation CAREER Award (Grant No. ECS 0543867).

[1] E. S. Snow, J. P. Novak, P. M. Campbell, and D. Park, Appl. Phys. Lett. **82**, 2145 (2003).
[2] V. C. Moore, M. S. Strano, E. H. Haroz, R. H. Hauge, R. E. Smalley, J. Schmidt, and Y. Talmon, Nano Lett. **3**, 1379 (2003).
[3] M. S. Arnold, A. A. Green, J. F. Hulvat, S. I. Stupp, and M. C. Hersam, Nat. Nanotechnol. **1**, 60 (2006).
[4] P. Beecher, P. Servati, A. Rozhin, A. Colli, V. Scardaci, S. Pisana, T. Hasan, A. J. Flewitt, J. Robertson, G. W. Hsieh, F. M. Li, A. Nathan, A. C. Ferrari, and W. I. Milne, J. Appl. Phys. **102**, 043710 (2007).
[5] Y. X.Zhou, H. Liangbing, and G. Gruner, Appl. Phys. Lett. **88**, 123109 (2006).
[6] M. A. Meitl, Z. Yangxin, A. Gaur, J. Seokwoo, M. L. Usrey, M. S. Strano, and J. A. Rogers, Nano Lett. **4**, 1643 (2004).
[7] S. H. Hur, C. Kocabas, A. Gaur, O. O. Park, M. Shim, and J. A. Rogers, J. Appl. Phys. **98**, 114302 (2005).
[8] S. H. Hur, O. O. Park, and J. A. Rogers, Appl. Phys. Lett. **86**, 243502 (2005).
[9] A. D. Pasquier, H. E. Unalan, A. Kanwal, S. Miller, and M. Chhowalla, Appl. Phys. Lett. **87**, 203511 (2005).
[10] M. W. Rowell, M. A. Topinka, M. D. McGehee, H. J. Prall, G. Dennler, N. S. Sariciftci, L. B. Hu, and G. Gruner, Appl. Phys. Lett. **88**, 233506 (2006).
[11] J. Li, L. Hu, L. Wang, Y. Zhou, G. Gruner, and T. J. Marks, Nano Lett. **6**, 2472 (2006).
[12] E. Artukovic, M. Kaempgen, D. S. Hecht, S. Roth, and G. Grüner, Nano Lett. **5**, 757 (2005).
[13] S. J. Kang, C. Kocabas, T. Ozel, M. Shim, N. Pimparkar, M. A. Alam, S. V. Rotkin, and J. A. Rogers, Nat. Nanotechnol. **2**, 230 (2007).
[14] J. A. Misewich, R. Martel, P. Avouris, J. C. Tsang, S. Heinze, and J. Tersoff, Science **300**, 783 (2003).
[15] A. Star, Y. Lu, K. Bradley, and G. Grüner, Nano Lett. **4**, 1587 (2004).
[16] J. Chen, V. Perebeinos, M. Freitag, J. Tsang, Q. Fu, J. Liu, and P. Avouris, Science **310**, 1171 (2005).
[17] E. S. Snow, F. K. Perkins, E. J. Houser, S. C. Badescu, and T. L. Reinecke, Science **307**, 1942 (2005).
[18] P. G. Collins, M. S. Arnold, and P. Avouris, Science **292**, 706 (2001).
[19] B. J. Landi, H. J. Ruf, J. J. Worman, and R. P. Raffaelle, J. Phys. Chem. B **108**, 17089 (2004).
[20] T. J. McDonald, C. Engtrakul, M. Jones, G. Rumbles, and M. J. Heben, J. Phys. Chem. B **110**, 25339 (2006).
[21] S. M. Bachilo, M. S. Strano, C. Kittrell, R. H. Hauge, R. E. Smalley, and R. B. Weisman, Science **298**, 2361 (2002).
[22] M. J. O'Connell, S. Sivaram, and S. K. Doorn, Phys. Rev. B **69**, 235415 (2004).
[23] D. W. Schaefer, J. Zhao, J. M. Brown, D. P. Anderson, and D. W. Tomlin, Chem. Phys. Lett. **375**, 369 (2003).
[24] H. Wang, W. Zhou, D. L. Ho, K. I. Winey, J. E. Fischer, C. J. Glinka, and E. K. Hobbie, Nano Lett. **4**, 1789 (2004).
[25] S. Badaire, P. Poulin, M. Maugey, and C. Zakri, Langmuir **20**, 10367 (2004).
[26] V. Nicolosi, D. Vrbanic, A. Mrzel, J. McCauley, S. O'Flaherty, C. McGuinness, G. Compagnini, D. Mihailovic, W. J. Blau, and J. N. Cole-

man, J. Phys. Chem. B **109**, 7124 (2005).
[27]H. E. Unalan, *Single Walled Carbon Nanotube Thin Films: Properties and Applications* (Rutgers University, Piscataway, NJ, 2006).
[28]M. Tory, *Sedimentation of Small Particles in a Viscous Fluid* (Computational Mechanics, Southampton, 1996).
[29]C. F. Bohren and D. R. Huffmann, *Absorption and Scattering of Light by Small Particles* (Wiley, Weinheim, Germany, 1998).
[30]Especially: $A_n(M,\zeta)=i\cdot\xi\cdot[\xi\cdot J_n'(\eta)\cdot J_n(\xi)-\eta\cdot J_n(\eta)\cdot J_n'(\xi)]$;
$B_n(M,\zeta)=\xi\cdot[M^2\cdot\xi\cdot J_n'(\eta)\cdot J_n(\xi)-\eta\cdot J_n(\eta)\cdot J_n'(\xi)]$;
$C_n(M,\zeta)=n\cdot\cos(\zeta)\cdot\eta\cdot J_n(\eta)\cdot J_n(\xi)\cdot(\xi^2/\eta^2-1)$;
$D_n(M,\zeta)=n\cdot\cos(\zeta)\cdot\eta\cdot J_n(\eta)\cdot H_n^{(1)}(\xi)\cdot(\xi^2/\eta^2-1)$;
$V_n(M,\zeta)=\xi\cdot[M^2\cdot\xi\cdot J_n'(\eta)\cdot H_n^{(1)}(\xi)-\eta\cdot J_n(\eta)\cdot H_n^{(1)\prime}(\xi)]$; and
$W_n(M,\zeta)=i\cdot\xi\cdot[M^2\cdot\xi\cdot J_n'(\eta)\cdot H_n^{(1)\prime}(\xi)-\eta\cdot J_n'(\eta)\cdot H_n^{(1)}(\xi)]$, where $\xi=x\cdot\sin(\zeta)$ and $\eta=x\cdot[M^2-\cos^2(\zeta)]$. $J_n$ and $J_n'$ are the first type Bessel functions and their derivatives with respect to $x$, respectively. $H^{(1)}$ indicate the Hankel functions.
[31]J. A. Fagan, J. R. Simpson, B. J. Landi, L. J. Richter, I. Mandelbaum, V. Bajpai, D. L. Ho, R. Raffaelle, A. R. H. Walker, B. J. Bauer, and E. K. Hobbie, Phys. Rev. Lett. **98**, 147402 (2007).
[32]See enclosed routines running in MATLAB™ 6.5. Routine CYLPARTD.M [similar to that presented by Bohren *et al.* (Ref. 29)] evaluate Eqs. (1)–(3) for normally oriented isotropic particles. Routine CYLPARTA.M evaluates Eqs. (1)–(3) by assuming a distribution of randomly oriented isotropic particles ($\zeta=0°-90°$). A comparison of the results achieved by these two routines allowed us to demonstrate that, for random distributions, the absorbance is mainly made up of particles normally oriented to the incident light which oppose the largest cross sectional area. Finally, we used the routine CYLPARTDANIS.M, in order to study the absolute and local minima of $Q_{ext}$ and $A$, by assuming cylindrical anisotropic particles. Complex refractive indices $N_{\|}(655\ \text{nm})=1.7+i0.7$ and $N_{\|}(655\ \text{nm})=3.5+i2.5$ were used, as recently determined for HiPCO SWCNTs by Fagan *et al.* (Ref. 31).
[33]H. E. Unalan, G. Fanchini, A. Kanwal, A. Du Pasquier, and M. Chhowalla, Nano Lett. **6**, 677 (2006).
[34]N. Pimparkar, J. Guo, and M. A. Alam, IEEE Trans. Electron Devices **54**, 637 (2007).
[35]R. Seidel, A. P. Graham, E. Unger, G. S. Duesberg, M. Liebau, W. Steinhoegl, F. Kreupl, W. Hoenlein, and W. Pompe, Nano Lett. **4**, 831 (2004).
[36]C. Kocabas, N. Pimparkar, O. Yesilyurt, S. J. Kang, M. A. Alam, and J. A. Rogers, Nano Lett. **7**, 1195 (2007).
[37]M. S. Fuhrer, J. Nygard, L. Shih, M. Forero, Y. Young-Gui, M. S. C. Mazzoni, C. Hyoung Joon, I. Jisoon, S. G. Louie, A. Zettl, and P. L. McEuen, Science **288**, 494 (2000).